The influences of the multi-scale sea surface temperature anomalies in the North Pacific on the jet stream in winter: Application of Liang-Kleeman information flow method and CAM5.3

Haibo HU[1], Yihang Zhao[1], Xiu-Qun Yang[1], Shunyu JIANG[2], Kefeng Mao[3], and Haokun Bai[1]

[1]Nanjing University
[2]Nanjing University of China
[3]National University of Defense Technology

January 20, 2023

Abstract

Using Climate Forecast System Reanalysis (CFSR) data and numerical simulations, the impacts of the multi-scale sea surface temperature (SST) anomalies in the North Pacific on the boreal winter atmospheric circulations are investigated. The basin-scale SST anomaly as the Pacific Decadal Oscillation (PDO) pattern, a narrow meridional band of frontal-scale smoothed SST anomaly in the subtropical front zone (STFZ) and the spatial dispersed eddy-scale SST anomalies within the STFZ are the three types of forcings. The results of Liang-Kleeman information flow method find that all three oceanic forcings may correspond to the winter North Pacific jet changing with the similar pattern. Furthermore, several simulations are used to reveal the differences and detail processes of the three forcings. The basin-scale cold PDO-pattern SST anomaly first causes negative turbulent heat flux anomalies, atmospheric cooling, and wind deceleration in the lower atmosphere. Subsequently, the cooling temperature with an amplified southern lower temperature gradient and baroclinity brings a lagging middle warming because of the enhanced atmospheric eddy heat transport. The poleward and upward development of baroclinic fluctuations eventually causes the acceleration of the upper jet. The smoothed frontal- and eddy-scale SST anomalies in the STFZ cause comparable anomalous jet as the basin-scale by changing the upward baroclinic energy and E-P fluxes. The forcing effects of multi-scale SST anomalies coexist simultaneously in the mid-latitude North Pacific, which can cause similar anomalous upper atmospheric circulations. This is probably why it is tricky to define the certain oceanic forcing that leads to specific atmospheric circulation variation in observations

Hosted file

essoar.10512720.1.docx available at https://authorea.com/users/531863/articles/620358-the-influences-of-the-multi-scale-sea-surface-temperature-anomalies-in-the-north-pacific-on-the-jet-stream-in-winter-application-of-liang-kleeman-information-flow-method-and-cam5-3

OBS: DJF: 1980-2009

3

4
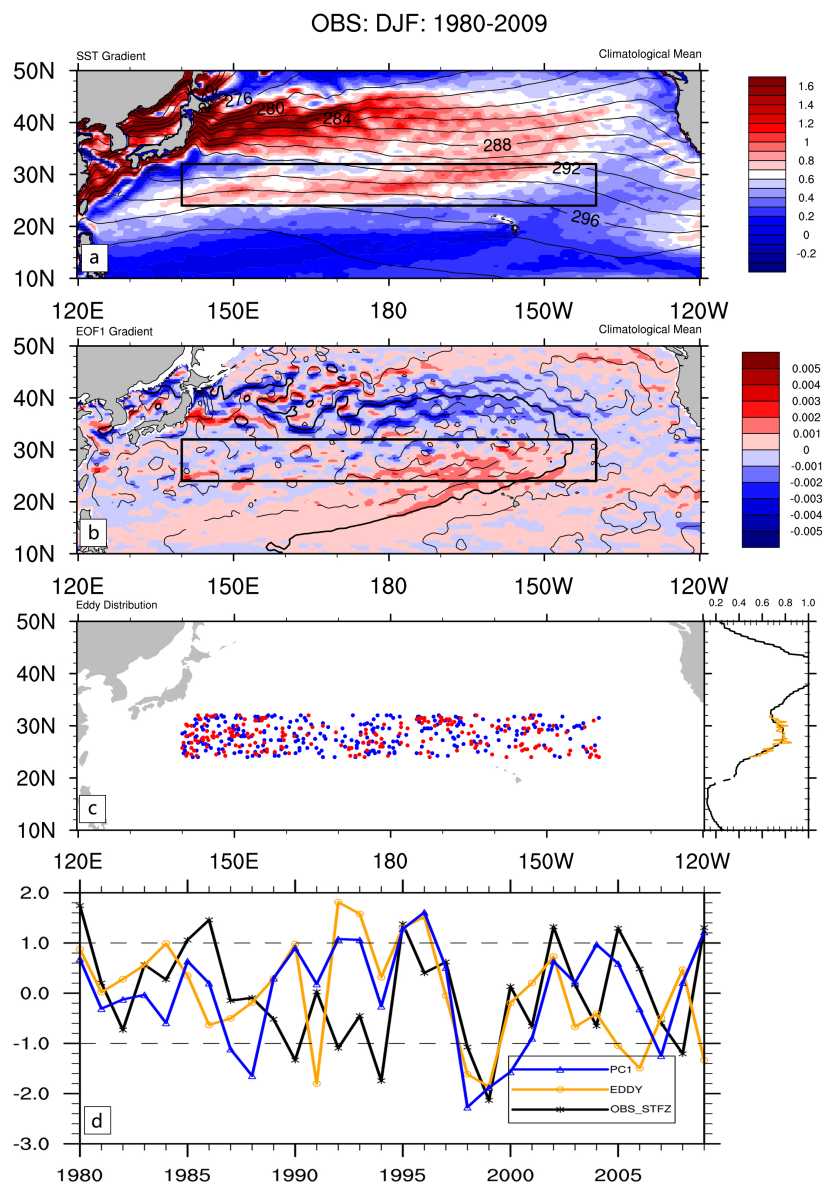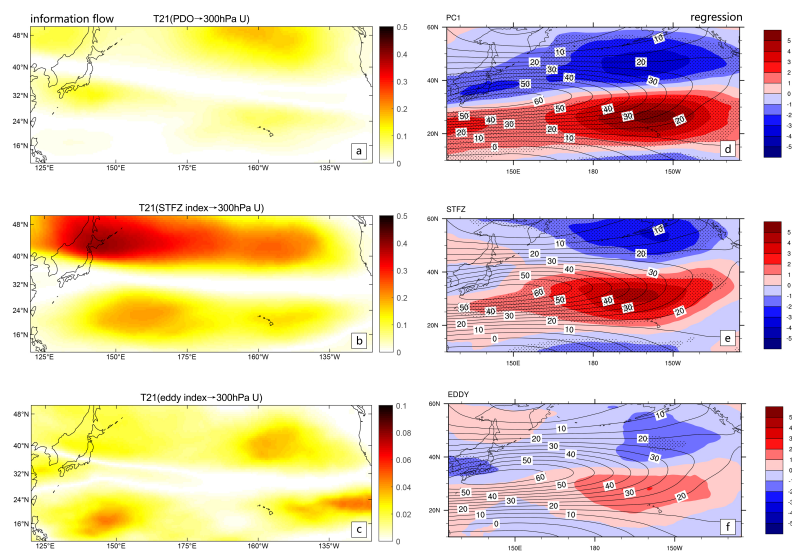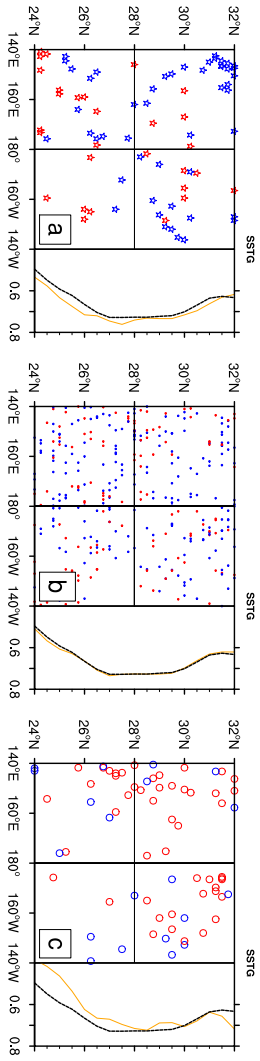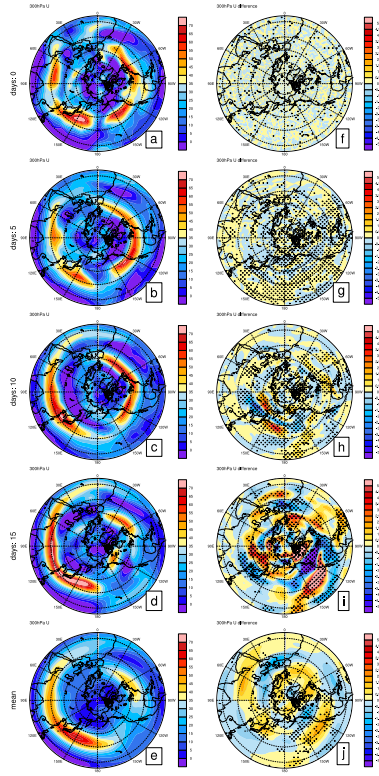
Haibo Hu[*], Yihang Zhao[*], Xiu-Qun Yang[*], Shunyu Jiang[*], Kefeng Mao[2], Haokun Bai[*]

[*]CMA-NJU Joint Laboratory for Climate Prediction Studies, Instituted for Climate and Global Change Research, School of Atmospheric Science, Nanjing University, Nanjing 210093, China

[2]National University of Defense Technology

Corresponding author: H.-B. Hu (huhaibo@nju.edu.cn)

Key Points:

- Basin-, frontal-, and eddy-scale oceanic forcing effects on the winter North Pacific jet exist simultaneously, which are of equal importance

- The feedback between the lower baroclinity and the upward and northward eddy heat transport dominates the basin-scale oceanic forcing effect

- Frontal- and eddy-scale SST anomalies in the STFZ cause comparable anomalous jet as the basin-scale by changing the upward E-P flux directly

Abstract

Using Climate Forecast System Reanalysis (CFSR) data and numerical simulations, the impacts of the multi-scale sea surface temperature (SST) anomalies in the North Pacific on the boreal winter atmospheric circulations are investigated. The basin-scale SST anomaly as the Pacific Decadal Oscillation (PDO) pattern, a narrow meridional band of frontal-scale smoothed SST anomaly in the subtropical front zone (STFZ) and the spatial dispersed eddy-scale SST anomalies within the STFZ are the three types of forcings. The results of Liang-Kleeman information flow method find that all three oceanic forcings may correspond to the winter North Pacific jet changing with the similar pattern. Furthermore, several simulations are used to reveal the differences and detail processes of the three forcings. The basin-scale cold PDO-pattern SST anomaly first causes negative turbulent heat flux anomalies, atmospheric cooling, and wind deceleration in the lower atmosphere. Subsequently, the cooling temperature with an amplified southern lower temperature gradient and baroclinity brings a lagging middle warming because of the enhanced atmospheric eddy heat transport. The poleward and upward development of baroclinic fluctuations eventually causes the acceleration of the upper jet. The smoothed frontal- and eddy-scale SST anomalies in the STFZ cause comparable anomalous jet as the basin-scale by changing the upward baroclinic energy and E-P fluxes. The forcing effects of multi-scale SST anomalies coexist simultaneously in the mid-latitude North Pacific, which can cause similar anomalous upper atmospheric circulations. This is probably why it is tricky to define the certain oceanic forcing that leads to specific atmospheric circulation variation in observations.

Key words: PDO; STFZ; multiple oceanic eddy spatial distributions; North Pacific upper jet

Plain Language Summary

The impacts of multi-scale interannual oceanic forcings on the winter North Pacific upper jet are studied such as the basin-scale Pacific Decadal Oscillation pattern SST anomaly, a narrow meridional band of frontal-scale smoothed SST anomaly in the subtropical front zone (STFZ) and the spatial dispersed eddy-scale SST anomalies within the STFZ. Using Liang-Kleeman information flow method, it is found that the above three oceanic forcings may change the upper jet over the North Pacific with the similar intensity and location characteristics. Further Community Atmosphere Model Version 5.3 simulations reveal that the basin-scale PDO-pattern cold SST anomaly firstly forces the lower atmosphere by the anomalous surface turbulent heat flux, which quickly brings air cooling and wind deceleration. After that, northward and upward eddy heat transports induced by temperature gradient south to SST anomaly cause atmospheric baroclinic variation and eventually lead to the acceleration of westerly upper jet over the cold SST. Differing the basin-scale anomaly, frontal- and eddy-scale SST anomalies in the STFZ directly change the uploading baroclinic waves and E-P fluxes divergence resulting in comparable atmospheric responses. This study will be beneficial to the weather and climate forecasts over the North Pacific and North America.

1 Introduction

Sea surface temperature (SST) anomalies of various spatial-temporal scales exist in the entire Pacific ocean-atmosphere system, such as the El Niño Southern Oscillation (ENSO) interannual event with temperature anomaly centered in the tropical Pacific (Bjerknes, 1969), and the Pacific Decadal Oscillation (PDO) event with interannual to decadal temperature anomalies centered in the North Pacific (Mantua et al., 1997). These two represent anomalous events are considered to have important impacts on global climate (Philander, 1983; Jin, 1997; Larkin and Harrison, 2002; Mantua and Hare, 2002), and both are closely related to local ocean-atmosphere interactions (Wu and Liu, 2003). Different from the tropical Pacific, the ocean-atmosphere coupling process is more complicated in the mid-latitudes of the North Pacific (Namias, 1969). The complexity is mainly due to the fact that besides the large-scale SST anomaly mode like the PDO pattern (Mantua et al., 1997), two banded SST gradient fronts (Nakamura et al., 1997; Wang et al., 2019; Chen et al., 2019) and widespread oceanic eddies (Chelton et al. 2007; Hu et al., 2021) can not be ignored for the effects on the upper mid-latitude atmosphere. At present, the similarities and differences of these multi-scale SST anomalies in the North Pacific and their connections have not been fully understood.

The most representative large-scale SST anomaly mode in the North Pacific is the PDO. It may be called the spatially ENSO-like mode of Pacific climate variability with longer period (Rasmusson and Wallace, 1983; Latif and Barnett, 1996). The PDO manifests as a large-scale cold (warm) SST anomaly in the mid-latitude North Pacific in winter, and the positive (cold SST anomaly) PDO phase corresponds to the intensification of the westerly jet in the upper

2

atmosphere (Mantua et al., 1997; Mantua and Hare, 2002). Some studies have pointed out that it is more like the mid-latitude westerly winds changing the latent heat flux of the sea surface, resulting in the basin-scale SST anomalies (Namias 1969; Palmer 1985; Deser et al. 1997; Miller and Schneider 2000). The mechanism of the PDO events has always been a research hotspot in mid-latitude ocean-atmosphere interaction. Many numerical experiments have emphasized that the PDO is the product of mid-latitude air-sea coupling (Hoskins and Karoly 1981; Kushnir and Held 1996; Newman et al., 2016, Wu and Liu, 2003). However, the direct observational evidence is vague (Mantua and Hare, 2002). Atmospheric forcing on the ocean has received much attentions (Hasselmann 1976; Battisti et al. 1995; Frankignoul et al. 1997), but which kind of mid-latitude SST anomalies leading to the large-scale anomalous atmospheric circulation remains an open question.

In addition to the basin-scale SST anomalies, there are two SST meridional gradient fronts zonally distributed in the North Pacific at least. One is the subarctic oceanic front with a great temperature gradient, the other is the Subtropical Frontal Zone (STFZ) locating near 28 to 32°N (Nakamura et al., 1997). The mid-latitude atmosphere has strong baroclinic properties, accompanied by the active development of synoptic eddies along the storm tracks and the generation of the Western Pacific Jet Stream (WPJS) (Ren et al., 2010; Chu et al., 2013). Various model simulations show that the forcing of frontal-scale SST anomalies in the oceanic frontal zones can propagates from the lower troposphere to the upper, and has indirect effects on atmospheric upper layer circulation (Nakamura et al., 1997; Feliks et al. 2004, 2007; Sampe et al. 2010; Yao et al. 2016, 2017; Wang et al., 2016, 2019). In particular, increment of the subtropical oceanic front intensity in winter will lead to the enhancement of the atmospheric storm tracks and WPJS in the mid-latitudes by altering the vertical propagation of baroclinic Rossby waves and the occurrence of barotropic Rossby wave breaking events (Wang et al., 2016, 2019; Chen et al., 2019).

Meanwhile, numerous mesoscale oceanic eddies distributed in the North Pacific. Previous studies have emphasized the impacts of isolated strong oceanic eddies on the local lower atmosphere, with regard to sea surface wind speed, boundary layer height, sensible and latent heat fluxes, and local precipitation (Small et al., 2008; Ma et al., 2015; Xu et al., 2016). Some studies have also pointed out that the mesoscale SST anomalies, alike the distribution of oceanic eddies, has an influence on the atmospheric storm tracks and produces the remote basin-scale atmospheric response (Ma et al., 2015; Sun et al., 2018). Since Wen et al. (2020) shown that oceanic eddies in the North Pacific do not exist in isolation, but often appear in the form of eddy pairs. Hu et al. (2021) used reanalysis data to give the difference between the effects of isolated oceanic eddies and eddy pairs on the upper atmospheric boundary layer. Subsequently, their work revealed that there is a close relationship between the spatial distributions of multiple oceanic eddies in the STFZ and the interannual variation of the observed STFZ intensity by changing the upward atmospheric baroclinic waves from the lower atmosphere to the middle and upper layers. However, in the mid-latitude North Pacific

air-sea coupling system, the multiple oceanic eddies exist simultaneously with the basin- and frontal-scale SST anomalies. The differences and connections between them are worth discussing.

In the observed North Pacific ocean-atmosphere system, due to the simultaneous oceanic anomalies of various temporal and spatial scales and the possible feedback processes with the upper atmosphere, it is difficult to determine the certain forcing source only by diagnosing the observational data. Numerical experiments have been used in previous studies on the North Pacific air-sea interaction (Kushnir and Lau, 1992; Kushnir and Held, 1996; Peng and Whitaker, 1999). However, different atmospheric general circulation model (AGCM) numerical experiments have found the inconsistent forcing results of the basin-scale PDO-pattern cold SST anomaly in the North Pacific on the WPJS (Liu, 2012). Some found linear baroclinic response with a sea surface low downstream of the warm SST anomaly (Yulaeva et al. 2001; Sutton and Mathieu 2002), while others produced an equivalent barotropic high downstream of the warm SST anomaly (Liu and Wu, 2004). Previous studies have shown that by enhancing the simulation capabilities of ocean eddies in numerical models, the forecast of extratropical cyclones and storm systems over the North Pacific in winter can be improved (Ma et al., 2015, 2017; Szunyogh et al., 2021), but the specific mechanism remains to be revealed. From the review, in the mid-latitude North Pacific Ocean, there are complex phenomena of multi-scale SST anomalies, such as the basin-scale PDO-pattern SST anomaly, the frontal-scale smoothed SST with STFZ intensity anomalies, and the eddy-scale SST anomalies with the spatial distribution of oceanic eddies. It is difficult to obtain their respective direct forcing effects on the upper atmospheric circulation by observation and reanalysis, and the existing numerical research results are inconsistent. In particular, similar to the studies that emphasized the effects of STFZ on baroclinity in the lower atmosphere, the basin-scale PDO-pattern SST anomaly is also accompanied by a significant meridional SST gradient. How to understand the atmospheric circulation responses considering the coexistence of SST and SST gradient anomalies in PDO events? What role does the spatial distribution of oceanic eddies play during different basin-scale PDO phase years? What are the differences and connections between the anomalies of basin-scale SST, frontal-scale oceanic smoothed front intensity, and the eddy-scale spatial distribution of oceanic eddies forcing on the upper atmosphere?

Based on the above questions, this paper is organized as follows. Section 2 introduces the data, methods and observations of North Pacific oceanic anomalies accompanied by atmospheric responses. Section 3 shows model introduction and experiment designs. Section 4 examines the detail forcing establishment process of basin-scale SST with obvious southern gradient anomalies on the upper atmosphere. Section 5 discussed the forcing mechanisms of smoothed frontal-scale subtropical oceanic front and eddy-scale oceanic eddy distributions on the atmosphere in winter. Summary and discussion are presented in Section 6.

2 Data, Methods and Observations of North Pacific Ocean Anomalies Accom-

4

panied by Atmospheric Responses

In this study, we used atmosphere and ocean reanalysis outputs of Climate Forecast System Reanalysis (CFSR) data in winter (DJF, i.e., Dec., Jan. and Feb.) from 1979 to 2009. This global, coupled and high-resolution product provided by the National Centers for Environmental Prediction (NCEP) has long been credited for its accurate estimation of the atmosphere and the ocean (Xue et al. 2011; Carvalho et al. 2012; Ma et al. 2015). The CFSR has the 6-hourly time resolution and the $0.5° \times 0.5°$ spatial horizontal resolution. The CFSR oceanic outputs have 40 levels from 5-m to 4478-m, in which top 20 levels are used in this study covered from ocean surface (5-m) to 205-m. The CFSR atmospheric outputs have multiple vertical coordinates. 300 hPa zonal wind is used in our study to investigate upper atmosphere. CFSR 6-hourly earth-system reanalysis outputs with the $0.5° \times 0.5°$ spatial resolution should be enough to detect oceanic eddies since the large eddies in this region have a typical mean eddy diameter of 200 km (see Fig. 3c in Chelton et al. 2007). Furthermore, to catch more details of approximate oceanic eddy center and moving locus, the spatial horizontal resolution is bilinearly interpolated to $0.25° \times 0.25°$ in this study, such as the Wen et al. (2020). All the correlation analysis and eddy composited analysis use daily mean of the 6-hourly outputs.

Liang–Kleeman information flow and time series causal analysis are used. In recent years, Liang (2014) has made a breakthrough in this issue using the Liang–Kleeman information flow theory. Information flow is considered a measure of causality, and the exchange between two events as information not only indicates the quantity, but also indicates the direction of the causal relationship (Liang 2015, 2016). The formalism bridges the gap between theory and real applications, and has been put to application with success to real world problems, such as the research on the relationship between carbon dioxide and global warming (Liang 2013; Stips et al. 2016; Liang 2018; Jiang et al., 2019).

To study the coupled air-sea interactions in the mid-latitudes of the North Pacific, it is important to reveal the process by which the complex oceanic anomalies affect the atmosphere. Based on previous studies, Fig. 1 shows three types of oceanic anomalies in the CFSR data, in which Fig. 1a shows the climate-averaged SST gradient, while the subtropical SST front can be determined by the visible large values area (black box) of SST gradient. Fig. 1b shows the first mode spatial pattern (PDO-pattern SST) and gradient obtained from the empirical orthogonal function (EOF) analysis of the annual average SST field in boreal winter. It can be seen that the basin-scale PDO-pattern SST is also accompanied by the large value of SST gradient, but located further southly than the subtropical oceanic temperature front. Fig. 1c shows the distribution of ocean eddies in the STFZ. The eddy detection dataset follows the study of Hu et al. (2021). From the zonally averaged SST gradient in the STFZ and eddy temperature gradient zonal mean lines, it can be seen that the distribution of ocean eddies has caused the same large SST gradients similar to subtropical SST gradient front. Therefore, since the three types of ocean anoma-

lies all have sea temperature gradients that can affect the upper atmosphere, it is necessary to discuss their accompanying atmospheric circulation anomalies separately. The EOF first mode (EOF1) time series (PC1) characterizing the basin-scale PDO-pattern SST change, the STFZ index characterizing the frontal-scale STFZ intensity change, and a newly defined ocean eddy index time series are respectively normalized and shown in Fig. 1d. Following the study of Hu et al. (2021), the uneven distribution of ocean eddies from north to south can cause a spatial dispersed eddy-scale SST gradient and then affect the middle and upper atmosphere. We define an ocean eddy index as the meridional deviation trend of anisotropic eddies from the main axis of the STFZ (28°N), which can characterize the strength of SST gradient anomaly generated by oceanic eddies. The definition is as follows

$$Eddy\ index = \sum_{i=1}^{n} \zeta_{ci} \cdot (\varphi_{ci} - 28) + \sum_{j=1}^{m} \zeta_{aj} \cdot (\varphi_{aj} - 28)$$

Among them, n and m are the number of cyclonic and anticyclonic eddies, respectively. ζ_c and ζ_a are the vorticity of the centers of cyclonic and anticyclonic eddies, respectively. And φ_c and φ_a are the latitudes where the eddy centers are located. When the eddy index is positive, it means that the cyclonic (anticyclonic) eddies within the STFZ are more inclined to the north (south), which is conducive to the positive anomaly of the SST gradient in STFZ. Fig. 1d shows that the time series of the three types of oceanic anomalies have obvious interannual intensity changes. The pairwise correlations of the three indices are calculated as r (PC1, EDDY) = 0.05, r (PC1, STFZ) = 0.41, r (EDDY, STFZ) = 0.51. It can be found that the basin-scale PDO-pattern and eddy-scale SST anomaly distributions are related to the frontal-scale STFZ intensity variation with significant positive correlations, while the PDO-pattern SST has no correlation with the eddy distribution. It is also worth noting that the PDO, generally described as inter-decadal cyclical variation, also exhibits significant

inter-annual variation within the selected 30 years.
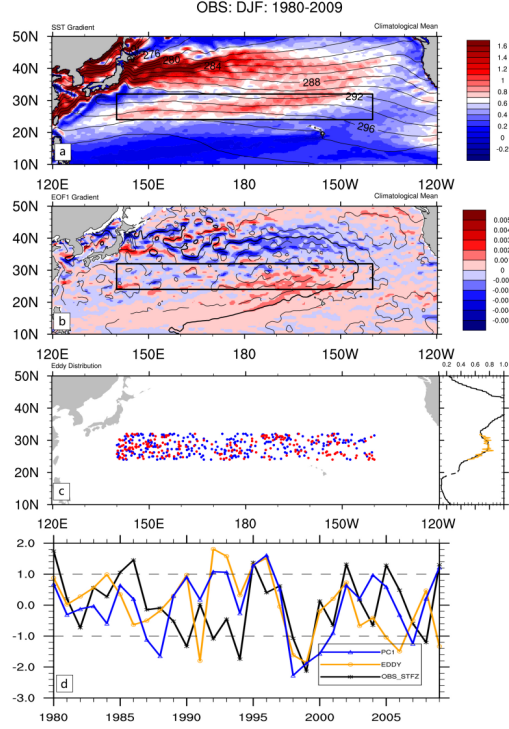
Figure 1. (a) North Pacific SST (contours, units: K) and SST gradient (shadings, units: $K \cdot degree^{-1}$) are in the climatological mean state. (b) The first mode spatial pattern is from the EOF analysis of the North Pacific winter SST annual series (EOF1, contours) and its gradient given in shadings. (c) Distribution of oceanic eddies is given in scatter plots (cyclonic eddies in blue and anticyclonic eddies in red) and mean SST gradient (black, units: $K \cdot degree^{-1}$) and eddy SST gradient within the STFZ (orange) are zonally averaged in line graph. (d) Line chart of standardized PC1 corresponding to EOF1 time series (blue), eddy index time series (orange) and observed STFZ index time series (black). Among them, the STFZ region is marked with a black box in (a, b).

In order to verify whether the ocean eddy index we defined can represent the strength of the spatial dispersed eddy-scale SST gradient anomaly caused by oceanic eddies, we define the significant strong eddy years with the eddy index higher than one standard deviation (1984, 1990, 1992, 1993, 1995, 1996), the significant weak eddy index years below one standard deviation (1991, 1998, 1999, 2005, 2006, 2009), and the normal rest years (detail years in Supplementary Table S1). Fig. 2 shows the characteristics of eddy distribution and SST gradient in different years. Fig. 2a shows that in strong eddy index years, more cyclonic eddies tend to the northern STFZ, and the zonally average SST gra-

7

dient increases, i.e., the intensity of the subtropical front strengthened. In the weak eddy index years, more anticyclonic eddies tend to the north of the STFZ. The zonal average SST gradient decreases, and the intensity of the subtropical front weakens. The results show that the eddy index can better describe the anomaly of the SST gradient caused by the characteristics of the multiple eddy distributions.
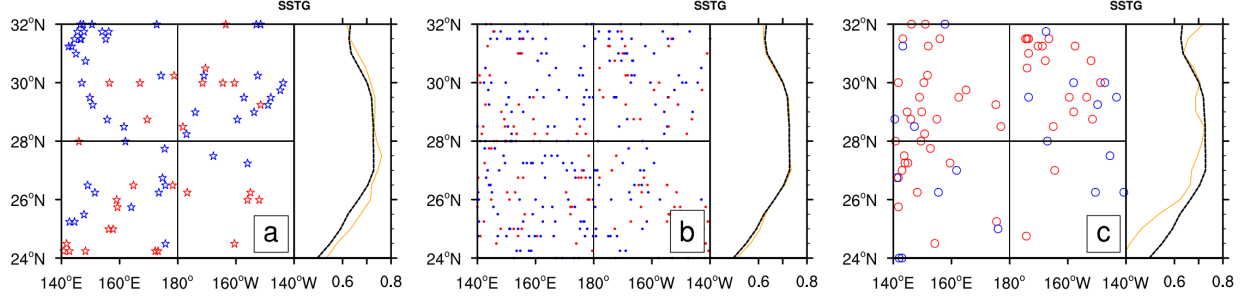
Figure 2. Ocean eddy distribution is given in scatter plots (cyclonic eddies in blue, anticyclonic eddies in red) and SST gradients are zonally averaged in strong (a), normal (b), and weak (c) years of the eddy index (line chart, units: $K \cdot degree^{-1}$, the black dotted lines are the climatological mean of the SST meridional gradient, and the orange solid lines are the zonal-mean SST gradient values caused only by oceanic eddies in the corresponding years).

In the coupled air-sea interaction, the ocean temperature gradient plays an important role in the forcing on the upper atmosphere. We found three types of ocean anomalies related to the SST gradient above, each of which has an interannual-scale intensity variation. Therefore, it is necessary to discuss the relationship between the three and their accompanying atmospheric circulation anomalies. Using the Liang–Kleeman information flow method, Figs. 3a-c shows the causal relationship between PC1 corresponding to the basin-scale PDO-pattern SST, frontal-scale STFZ intensity, the eddy index and the atmospheric 300hPa zonal wind speed. The results show that all three types of ocean anomalies can cause abnormal changes in the upper atmospheric circulation. Their regression analyses show similar results (Figs. 3d-f). All three oceanic forcings can affect the upper zonal wind field. Especially the acceleration on the right side downstream of the jet axis, where the basin-scale PDO-pattern SST has the most significant impact on the atmosphere. A relatively weak mathematical statistical relationship exists between the upper wind and eddy index. The observed jet response obtained by composition analysis shows similar results (Supplementary Figure S1). However, in the real world ocean-atmospheric system, the three types of oceanic anomalies coexist. It is difficult to diagnose their respective atmospheric responses through observational data. Whether these three types of ocean anomalies all have forcing on the upper atmosphere, and what are the differences and connections between them? It is necessary to

use numerical models to further reveal the above questions.
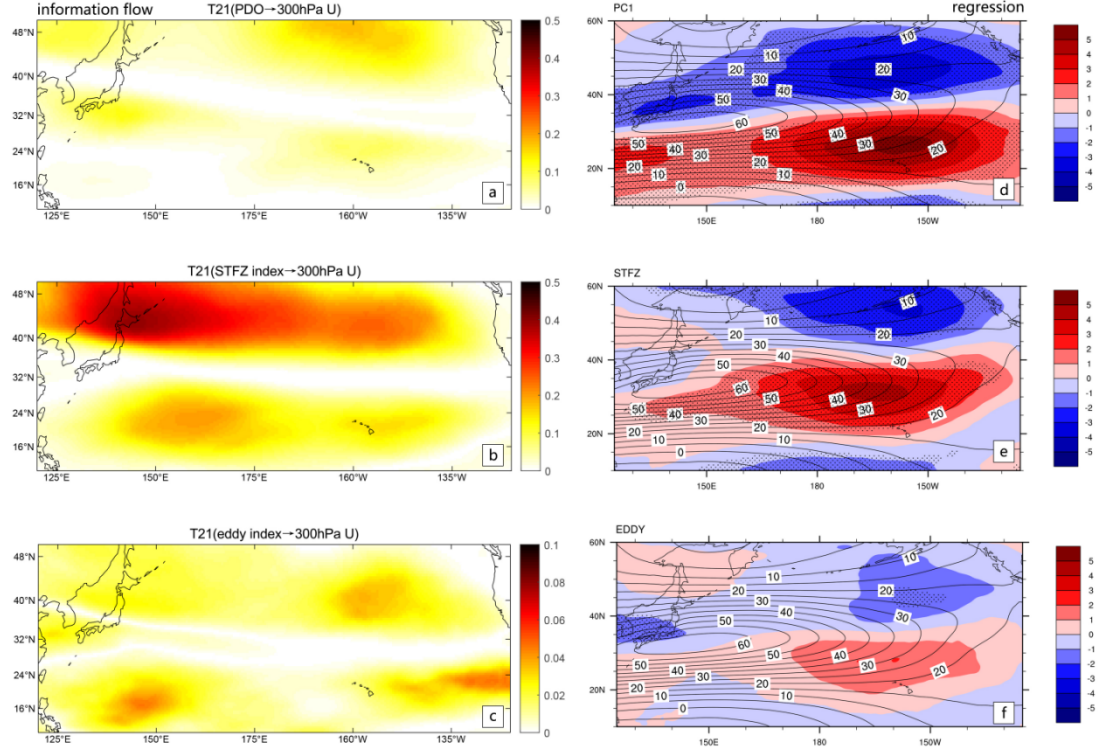
Figure 3. Liang-Kleeman information flow (a-c) and regression analysis (d-f, shadings) are conducted to the (a, d) PDO-pattern SST PC1 series, (b, e) STFZ index and (c, f) eddy index with observed 300 hPa zonal wind. Climatological mean zonal wind field on 300 hPa is represented by contours (units: $m \cdot s^{-1}$) in (d-f). The shadings (a-c) and dotted areas (d-f) pass the 95% significance, respectively.

3 Model Introduction and Experiment Design

The Community Atmosphere Model Version 5.3 (CAM5.3) of the National Center for Atmospheric Research (NCAR) is used in this study (Neale et al. 2010; Gent et al. 2011). CAM5.3 is the latest in a series of global atmosphere models and contains same notable improvements. In addition, CAM 5.3 also includes the Land Surface Module CLM4.5, which provides atmospheric conditions with land boundary conditions and lower boundary conditions such as energy, momentum and water vapor exchange between land and air (Oleson et al. 2010). The horizontal resolution of the model used in this paper is T85 (128×256, about 1.5°). The -p hybrid coordinates are taken in the vertical direction. The coordinates are used in the near ground layer. The -p transition coordinates are used in the middle, and the upper layer is the pure p coordinate, covering

9

26 layers. The deep convection process is processed using a parametric scheme developed by Zhang and McFarlane (1995) and corrected by the increased flow transport of Richter and Rasch (2008). Compared with previous version, the default power core of CAM5.3 has been changed from the original spectral core to a finite volume core. CAM5.3 has also significantly improved on deep convection scheme, Arctic cloud simulation, radiated interface and computational scalability. It also improves simulation capabilities for ENSO (Neale et al. 2008). Several control and sensitivity experiments are designed to understand the effects of basin-scale PDO-pattern SST anomaly, total SST anomalies in STFZ, frontal-scale smoothed SST anomaly and the spatial dispersed eddy-scale SST anomalies within the STFZ, which are listed in Table 1. The CTRL Simulations run from December 1, 1979 to February 28, 2010 with output every 5 days for 31 consecutive years. The CTRL output on December 1 of each simulation year provides the unified year-by-year winter initial fields for all the subsequent sensitivity experiments.

Experiment	Description of the forcing fields
CTRL	Excluding SST, all forcing fields are fixed to the values in year 2000. The SST forcing is
CTRL_NoNP	All parameterization schemes and forcing are the same as CTRL, but the SST forcing is
EXP_PDO	Same as CTRL_NoNP, but the North Pacific SST forcing has the interannual variability
EXP_AllSTFZ	Same as CTRL_NoNP, but the SST forcing adds the observed total interannual SST on
EXP_FrontSTFZ	Same as CTRL_NoNP, but the SST forcing adds the interannual anomalous observed S
EXP_EddySTFZ	Same as CTRL_NoNP, but the SST forcing adds the interannual spatial filtering anoma
EXP_PDO+Eddy	Same as CTRL_NoNP, but the SST forcing is the SST anomaly in EXP_PDO adds the

Table 1. Experiment designs.

The North Pacific is defined as 10°N-50°N, 140°E-140°W in CTRL_NoNP and EXP_PDO. Using climatology to exclude interannual variability, the model runs a 30-year discrete winter simulation from December 1, 1980 to February 28, 2010. The initial of each CTRL_NoNP simulation was the output on the day of the CTRL. The 30 winters simulations were the responses of the mid-latitude atmosphere to the climatological North Pacific temperature, which are used for the comparisons of the sensitivity experiments below. For EXP_PDO, the difference between the ensemble average of 17 PDO positive phase (cold SST) events (detail years in Supplementary Table S1) and CTRL_NoNP is regarded as the impact of the interannual basin-scale PDO-pattern cold sea temperature anomalies on atmospheric circulation in mid-latitudes.

The subtropical frontal zone (STFZ) is defined as 24°N-32°N, 140°E-140°W in EXP_AllSTFZ, EXP_FrontSTFZ and EXP_EddySTFZ. The difference between the ensemble average of 15 events in EXP_AllSTFZ with a positive STFZ index in 30 years and CTRL_NoNP is regarded as the effects of the overall STFZ meridional gradient enhancement (including frontal- and eddy-scale anomalies) on the mid-latitude atmospheric circulation. For EXP_FrontSTFZ

(frontal-scale anomalies), the difference between the ensemble average of 15 events with a positive smoothed meridional SST gradient index over 30 years and CTRL_NoNP is the impact of only oceanic front enhancement without eddy forcing in the STFZ on the mid-latitude atmospheric circulation. For EXP_EddySTFZ (eddy-scale anomalies), the difference between the ensemble average of 16 winters with a positive STFZ index and CTRL_NoNP is the impact of only spatial dispersed eddy-scale SST anomalies within the STFZ on the mid-latitude atmospheric circulation. For EXP_PDO+Eddy, the differences between 4 (1) eddy enhancement winters under the background of positive (negative) PDO phase years and CTRL_NoNP show the effects of eddy-scale SST anomalies within the STFZ on atmospheric circulation over the North Pacific, considering the different basin-scale PDO phase backgrounds. All Detailed positive (negative) event years of each experiment are listed in Supplementary Table S1.

The amplitudes of all SST anomalies perform a cosine function that decreases outward from the center of the region, ensuring the spatial continuity of the overall temperature and temperature gradient in the Pacific Ocean (Chen et al., 2019). We first verified and evaluated the validity and reliability of the model for simulating the atmospheric circulation in winter through control simulations (CTRL). The SST and SST gradient fields in the simulations and the 300 hPa zonal wind response field are basically consistent with the observational results (Supplementary Figure S2), which proves that the CAM5.3 atmospheric general circulation model can be used to conduct subsequent series of sensitivity experiments on the effects of basin-, frontal-, and eddy-scale SST anomalies on atmospheric jets.

4 The forcing effects of basin-scale PDO-pattern SST and SST gradient anomalies on the upper atmosphere

The basin-scale PDO spatial pattern SST is the main mode of the North Pacific SST anomaly, and the coupling relationship between the PDO-pattern SST and the atmospheric circulation anomaly is also a research topic that has received extensive attentions (Mantua et al., 1997; Mantua and Hare, 2002; Newman et al., 2016). However, the existing simulation studies have not been clear about the atmospheric response characteristics of PDO-pattern SST anomaly forcing, especially the mechanism (Yulaeva et al. 2001; Liu and Wu, 2004). In order to compare the forcing differences between the basin-scale SST anomalies and the subsequent frontal- and eddy-scale anomalies, we also conducted a set of cold SST experiments in positive phase years of the PDO (EXP_PDO in Table 1). The results of EXP_PDO show that the WPJS gradually builds up and strengthens from west to east in the winters of positive PDO phase (Figs. 4a–d). The simulated upper-level jet response reaches equilibrium after 15 days of simulation, and the location and intensity of the WPJS averaged in winter are consistent with the observations (Figs. 3d, 4e). To reflect the independent forcing process of the basin-scale PDO-pattern cold SST (excluding the effects of interannual variability in other ocean areas), we define the difference

between the EXP_PDO and CTRL_NoNP experiments as the forcing effect of the basin-scale SST anomaly. From the winter averaged response field, the upper atmosphere response to the cold PDO-pattern SST is mainly represented by the increase of the jet stream on the downstream of the climatological WPJS (Fig. 4j). Such a mean response starts from the 10 days of oceanic forcing (Fig. 4h), gradually intensifies northwestward (Figs. 4h-i), and finally stabilize to an equilibrium state in the third pentad (Fig. 4i). Except for the notable differences in wind fields over the North Pacific, the zonal wind in the middle and high latitudes of the entire northern hemisphere has actually changed. At present, this paper only focuses on the changes of the mid-latitude jet in the North Pacific region.
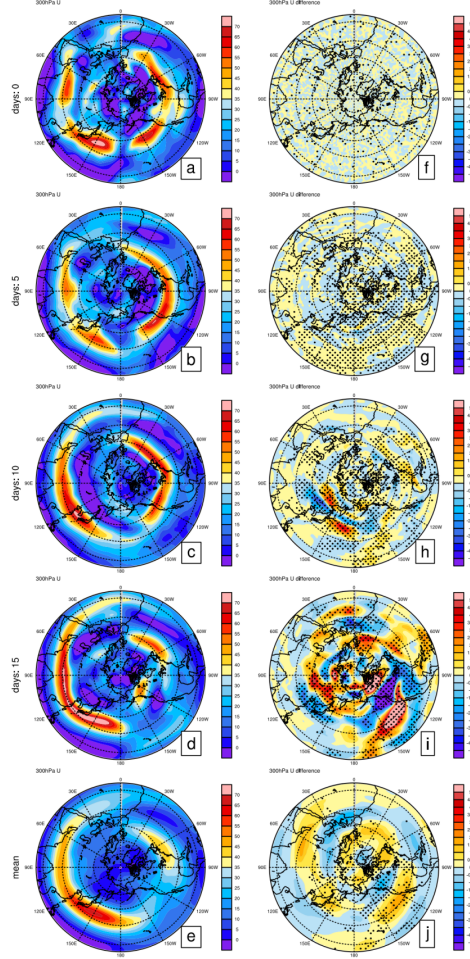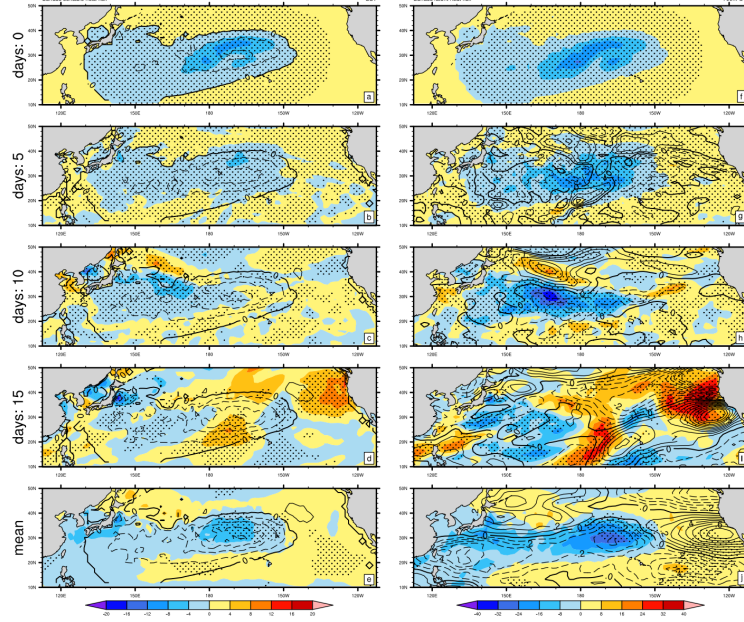

Figure 4. In response to the basin-scale PDO-pattern cold SST experiment,

(a-e) are the ensemble averaging (17 winters) simulations of day 0, 5, 10, 15 and winter mean of 300 hPa atmospheric zonal wind speed (units: $m \cdot s^{-1}$) in EXP_PDO. (f-j) are the 300 hPa atmospheric zonal wind speed anomalies (units: $m \cdot s^{-1}$) distinguished from CTRL_NoNP. The dotted areas passed the 95% significance t-test.

In order to clarify the forcing process that establish WPJS in the upper atmosphere in response to the basin-scale PDO-pattern SST anomaly, we first focus on the air-sea interface that is initially forced by SST. The annual mean sensible heat flux (Figs. 5a-d, shadings) and latent heat flux (Figs. 5f-i, shadings) of the positive phase are anomalous in-phase responses. It can be found that with increasingly colder SST forcing, in the first pentad, the turbulent heat flux is a negative anomaly corresponded with the cold sea temperature and the zonal wind deceleration in the lower atmosphere at 700 hPa (Figs. 5b, g). However, a positive anomalous heat flux opposite over the cold SST appeared in the second pentad, and there was a corresponding increase in the low-level zonal wind (Figs. 5c, h). Until the third pentad after the occurrence of SST forcing, a positive anomaly of the heat flux presents at the air-sea interface in the large-scale cold SST center (Figs. 5d, i), which suggests that the heat flux anomaly is not only forced by the sea temperature, but also receives feedback from the atmospheric temperature advection. The atmospheric 700 hPa zonal wind acceleration corresponding to the positive flux anomalies are also present (Fig. 5i, contours). Ultimately, the winter-averaged turbulent heat flux anomaly at the air-sea interface manifests as a negative anomaly in the cold SST center and a positive anomaly around it (Figs. 5e, j). This is inconsistent with the abnormal upward turbulent heat flux at the west and center of the PDO-pattern cold SST anomaly seen in our observations (Wang et al., 2019). The absence of atmospheric feedback forcing on SST in the AGCM may be a possible reason for it. However, the current spatial distribution of sea surface turbulent heat flux anomalies is corresponded with the simulated changes in the intensity of the upper jet, which shows as acceleration (deceleration) in the increase (decrease) of the sea surface turbulent heat flux under the cold advection. How the basin-scale cold PDO-pattern SST anomaly causes the acceleration of the lower

13

atmosphere and even the upper jet, the mechanism needs further discussion.

Figure 5. In response to basin-scale PDO-pattern cold SST anomalies, the ensemble averaging simulations of day 0, 5, 10, 15 and winter mean of (a-e) sea surface temperature anomalies (units: K) are given in contours, and the sensible heat flux anomalies (units: $W \cdot m^{-2}$) are shown in shadings (f-j) distinguished from CTRL_NoNP. The contours indicate atmospheric 700 hPa zonal wind anomalies (units: $m \cdot s^{-1}$), and shadings indicate latent heat flux anomalies (units: $W \cdot m^{-2}$). The dotted areas passed the 95% significance t-test.

The zonally-averaged atmospheric response is shown to investigate the influence of the PDO-pattern SST anomaly forcing from the lower layers upward (Fig. 6). Within 5 days, the lower atmospheric temperature cooling rapidly appearing over the basin-scale PDO-pattern cold SST (Fig. 6b, contours). Meanwhile, the zonal wind speed decelerates in middle and lower layer over cold SST anomaly south to 40°N yet accelerates northward. This is consistent with the response of the atmospheric thermal wind at the early stage of the SST anomaly emphasized in previous studies (Chen et al., 2019). However, the responded atmospheric wind at this time in our simulations shows a baroclinic structure with opposite results above and below 400 hPa (Fig. 6g, contours). Also, at the 5th day of simulation, due to the cooling of the atmosphere above the cold sea temperature, a relatively significant positive atmospheric temperature gradient anomaly (20°N) appeared in the lower atmosphere south of the cold sea temperature anomaly (Fig. 6b, shadings). The positive anomaly of the atmospheric temperature gradient caused the increase of baroclinity in the lower atmosphere (Fig. 6g). Subsequently, the enhanced atmospheric eddy activity caused the

warming of the atmosphere centered at 700 hPa above the cold sea temperature anomaly (30°N) in the second pentad (Fig. 6c, contour) with a stronger temperature gradient (40°N) on its north side (Fig. 6c, shadings). The strong temperature gradient was accompanied by an increase in baroclinity and an acceleration of zonal winds with an equivalent barotropic structure (Fig. 6h). Further atmospheric warming and stronger atmospheric baroclinity propagated to the upper atmosphere poleward (Figs. 6d, e, i, j). Meanwhile, the persistent PDO-pattern cold SST is maintaining the lower baroclinic anomaly. The subsequent enhanced poleward and upward atmospheric eddy heat transport and the intensified atmospheric warming complete a positive feedback. Ultimately, the atmospheric responses in positive PDO phases are atmospheric cooling over the cold SST forcing (Fig. 6e) and an increase jet at the northeast of the climatological WPJS (Figs. 5j and 6j). The key to the above forcing process is the southern sea surface temperature gradient accompanied by large-scale cold sea

temperature.
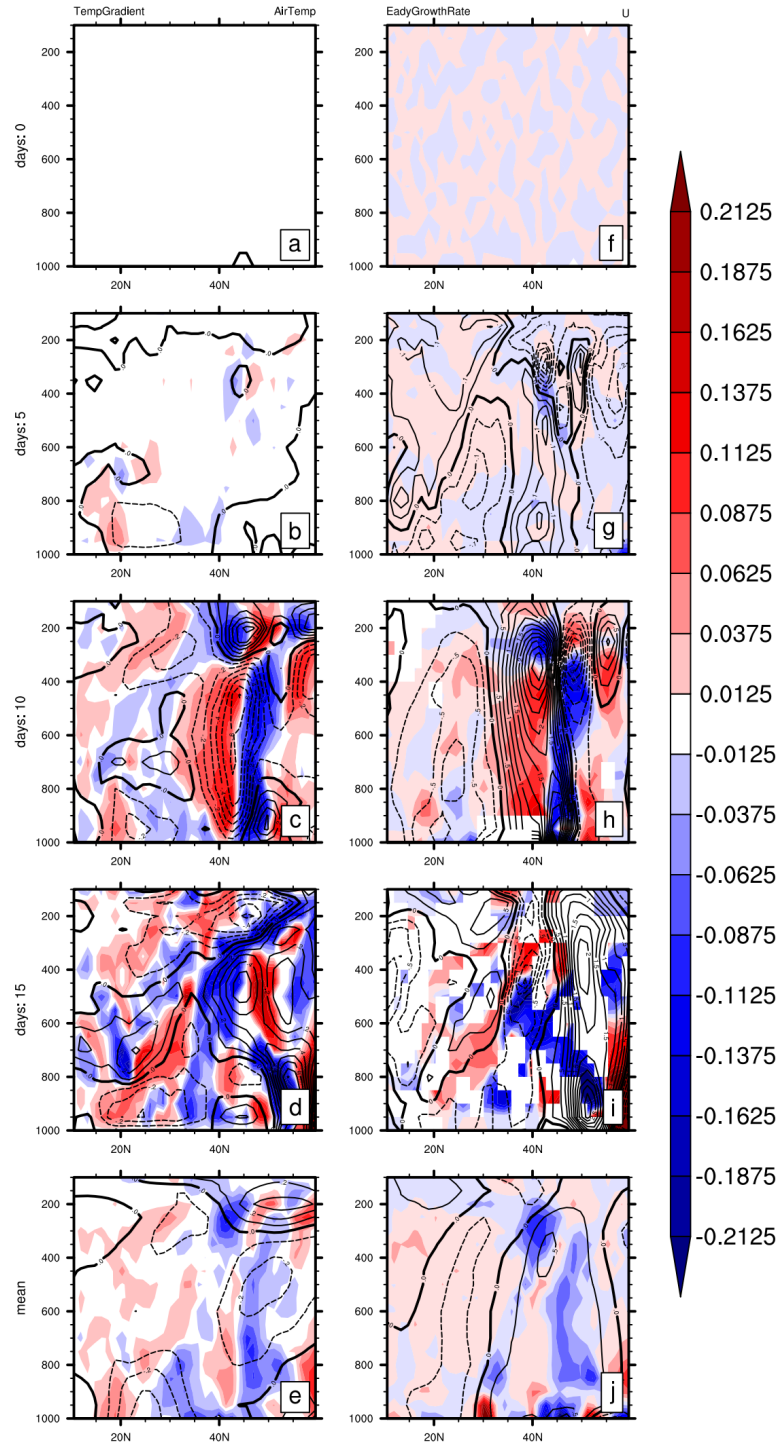
Figure 6. In PDO positive phase years, the ensemble averaging atmospheric response to the basin-scale PDO-pattern SST anomalies is given per 5 days and in winter mean. Among them, (a-e) contours indicate temperature anomalies (units: K), and shadings indicates temperature gradient anomalies (units: $K \cdot degree^{-1}$). Contours in (f-j) indicate atmospheric zonal wind anomalies (units: $m \cdot s^{-1}$), and shadings indicate anomalies in the Eady growth rate (units: $10^{-5} \cdot m \cdot s^{-2}$). Shadings areas pass the 95% significance t-test.

In order to verify the source of the abovementioned atmospheric warming that occurs over the cold SST after 10 days of the simulations. We calculated the atmospheric eddy heat transfer term, and the results are shown in Fig. 7. After the PDO cold SST forcing, in the first pentad near sea surface atmosphere is cooled by the cold SST forcing. At this time, there is no obvious meridional transport of atmospheric eddy heat in the cooling center (Fig. 7b). However, a significant temperature gradient and a positive baroclinic anomaly appear on the south side of the negative surface air temperature anomaly (Fig. 7f). At the 10th day, the atmosphere warmed up over the cold SST center at 700 hPa, which was due to the northward transfer and upload of heat caused by the baroclinic eddy activity at the southern lower atmosphere (Fig. 7c). A more pronounced atmospheric temperature gradient and baroclinity then appear on the northern side of the warmed atmosphere (Fig. 7g). Thereafter, further poleward transmission and upload of atmospheric warming triggered by similar atmospheric processes (Figs. 7d, h). The discussion in this section is the response of atmospheric circulation to the large-scale cold SST anomalies in the mid-latitude North Pacific in PDO positive phase years. The warm ocean surface in PDO

negative phases forces the atmosphere in almost the opposite way (not shown).
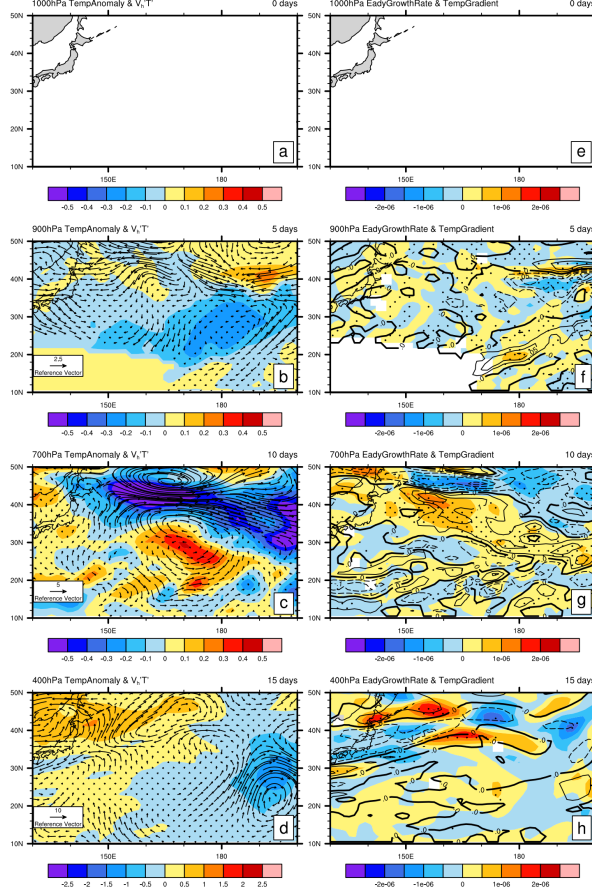
Figure 7. In response to the basin-scale PDO-pattern SST anomalies, the ensemble averaging anomalous atmospheric circulation and process are given from 1000 hPa to 400 hPa per 5 days. The arrows in (a-d) represent the heat transport of the atmospheric eddy activity (units: $K \cdot m \cdot s^{-1}$), and the shadings represent the abnormal temperature (units: K); (e-h) the contours represent the anomalies of the atmospheric temperature gradient (units: $K \cdot degree^{-1}$), and the shadings represent the abnormal Eady growth rate (units: $m \cdot s^{-2}$). The dotted areas passed the 95% significant test.

5 The forcing mechanisms of frontal- and eddy-scale SST anomalies in the STFZ on the winter atmosphere

In the previous section, the southern SST gradient dominants the forcing effect of the basin-scale PDO-pattern SST anomaly on atmosphere. The southern region of the basin-scale PDO-pattern SST anomaly is close to the STFZ high-

lighted in previous studies. In addition, insignificant differences exist between the southern meridional temperature gradient accompanied by the basin-scale PDO-pattern SST anomaly and the direct STFZ frontal intensity (Supplementary Figure S3). So, what about the direct forcing on the atmospheric circulation by the meridional temperature gradient of the individual STFZ? Is it similar to the basin-scale PDO-pattern SST anomaly forcing? Furthermore, Hu et al. (2021) revealed the relationship between the distribution characteristics of multiple oceanic eddies in the STFZ of the North Pacific and the changes in the intensity of the STFZ. Therefore, when studying the oceanic interannual variability in the STFZ region, it is necessary to further divide the total SST anomalies (EXP_AllSTFZ) into the effects of the spatial dispersed eddy-scale anomaly (EXP_EddySTFZ) and the frontal-scale SST anomalies (EXP_FrontSTFZ) after smoothing out the ocean eddies. The three differences between the above three sets of experiments and the CTRL_NoNP experiment can reflect the respective interannual forcing effects of the total STFZ intensity, smoothed frontal-scale and eddy-scale SST anomalies on the atmospheric circulation within the STFZ (Fig. 8). It can be found that all three forcings cause the band-shaped SST gradient large value area near 25°N, and all lead to the zonal-mean westerly acceleration centered at 30°N. Compared with the acceleration of upper jet (40°N in Fig. 6j) induced by the basin-scale PDO-pattern cold SST forcing, the changes of the jet stream in the three sets of experiments have a considerable variation range, but the location is more southerly. Notably, although the eddy-scale SST anomalies are the weakest, they caused the most significant westerly increases. Furthermore, the forcing effect of the total STFZ intensity change on the zonal-mean jet is not a simple linear superposition of frontal-scale and eddy-scale forcings.
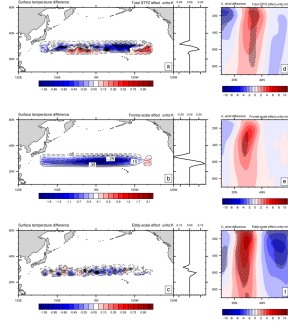
Figure 8. In response to the (a) total (frontal- and eddy-scale), (b) smoothed frontal-scale, and (c) eddy-scale SST anomalies in years with a strong meridional temperature gradient, the ensemble averaging sea surface temperature anomalies (Shadings, units: K), temperature gradient anomaly (contours, units: $K \cdot degree^{-1}$), zonal mean temperature gradient anomaly (black solid line on the right) are shown. The composited zonal wind (units: $m \cdot s^{-1}$) responses distinguished from CTRL_NoNP are in (d-f). The dotted areas passed the 95% significance t-test.

Although the above three sets of experiments have good agreement after zonal averaging, there is a big difference between the three in the east-west direction (Fig. 9). It can be found that the meridional temperature gradient value of the eddy-scale SST anomaly is generally small in the whole east-west direction in strong eddy index years. However, east of 180°, the meridional gradient values show relative larger positive anomalies, while negative on the west side (Fig. 9c). In the years of stronger SST meridional gradient value, the temperature gradient has more significant changes in the east-west direction for the total STFZ and smoothed frontal-scale SST anomaly experiments, especially for the total STFZ experiment (Figs. 9a, b). Though all the SST gradients show large values at 180°-140°W in the three experiments, the upper-air wind speed responses are different. The total STFZ effects show two accelerations upstream north and downstream south sides of WPJS (Fig. 9d). In response to smoothed frontal-scale SST anomaly, the wind anomalies show an overall acceleration along the jet axis from upstream to downstream, especially on the downstream (Fig. 9e). For the eddy-scale SST anomalies, although the meridional temperature gradient at this time is small, the downstream acceleration of the jet stream is of the same magnitude as the previous two sets of experiments. However, compared with the smoothed frontal-scale effect, the jet stream acceleration is more easterly in eddy-scale forcing simulations. The results may suggest the importance of the SST gradient east of 180°. However, there is no direct linear relationship between the response intensity of the jet and the temperature gradient anomaly. It is worth noting that although the zonal averaged meridional temperature gradient increment corresponds to the similar zonal-mean upper jet acceleration responses (Figs. 8e, f), the detail atmospheric westerly anomalies are at different locations in the east-west direction (Figs. 9e, f) for the smoothed frontal-scale and eddy-scale experiments. The jet response of the total STFZ experiment is more like the joint performances of the frontal- and eddy-scale SST anomalies. In addition, there is a negative SST gradient around 140W in the total and frontal-scale STFZ experiments (Figs. 9a, b), which is related to the north-east tilt of the STFZ (Wang et al., 2019).
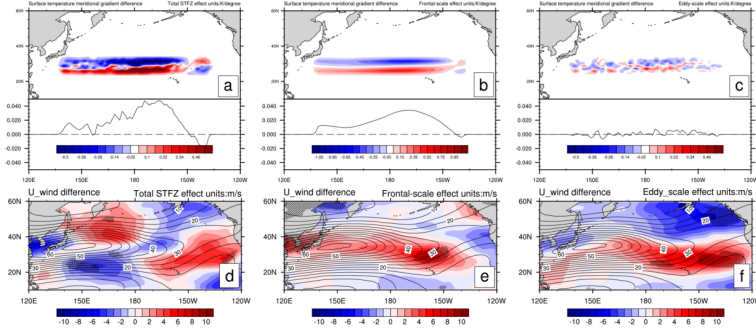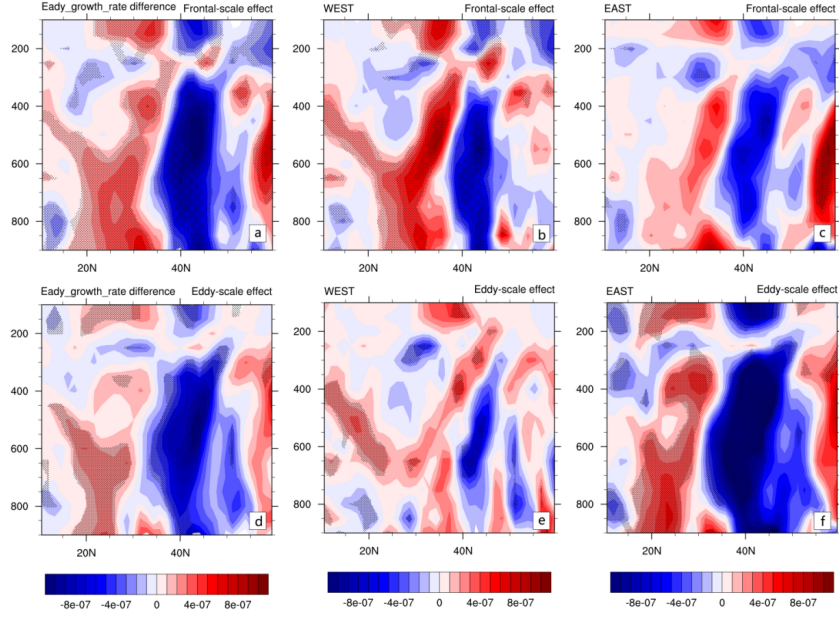

Figure 9. In response to the (a) total (frontal-scale and eddy-scale), (b) frontal-scale, and (c) eddy-scale SST anomalies in STFZ, the ensemble averaging sea

surface temperature gradient anomalies in strong eddy index years (Shadings, units: K · degree^{-1}), anomalous meridional mean of temperature gradient (black solid line) are shown and (d-f) give its corresponding 300 hPa atmospheric zonal wind anomaly (Shadings, units: m · s^{-1}) responses and CTRL_NoNP mean zonal wind is contoured (units: m · s^{-1}), the dotted areas passed the 95% significant t-test.

The baroclinity and Eady growth rate of the lower atmosphere are thought to be directly affected by the sea-surface meridional temperature gradient (Nakamura et al., 1997; Chen et al., 2019). Fig. 10 shows the zonal composite of the Easy growth rate of the two groups of experiments. Overall, both sets of experiments resulted in a significant zonal-mean baroclinic intensification in the lower atmosphere around 30°N (Figs. 10a, d). This increased baroclinity has a northward and upward transfer trend. Although there is no direct lower oceanic forcing, a weakened baroclinic adjustment in the atmosphere near 40°N generates to the north of the SST forcing zone. Significant differences are in the east-west direction between the forcing effects of the smoothed frontal- and eddy-scale SST anomalies on the baroclinity. West of 180°, the smoothed frontal-scale forcing effect is significantly stronger than that of the eddy-scale (Figs. 10b, e). East of 180°, the situation is reversed (Figs. 10c, f). Similarly, it can be seen that for the strong meridional temperature gradient events of the smoothed frontal-scale STFZ, upward wave flux anomaly exists at 30°N on the west side with significant local Eliassen-Palm flux (E-P flux, Trenberth, 1986) divergence and jet acceleration on middle-to-upper layers (Fig. 11b). However, on the eastern section, the forcing effects of the frontal-scale SST anomaly are mainly the rising E-P fluxes near 40°N and the downward E-P fluxes in the middle atmosphere near 30°N, which may be related to the negative anomaly of the eastern meridional SST gradient in Figs. 9a, b. For the eddy-scale forcing simulations, there is no significant baroclinic wave activity on the entire west section (Fig. 11e). However, significant uploading E-P flux, upper layer E-P divergence, and upper jet acceleration anomalies occur near 30°N on the east section (Fig. 11f). This chapter discusses the simulated forcing results of strong meridional gradient events in total STFZ changes, smoothed frontal-scale SST anomaly changes, and eddy-scale SST anomaly on the atmospheric circulation. The above numerical simulation results show that the spatially dispersed eddy-scale SST anomaly in the subtropical frontal area can lead to the similar zonal-mean response of the upper atmosphere circulation as the total STFZ effect. The difference in the spatial characteristics of the SST anomaly in the east-west direction leads to a more eastward acceleration of the atmospheric westerly jet caused by the eddy-scale anomaly. The total forcing effects of the SST anomalies in the STFZ on the winter atmospheric circulation can be understood as a joint manifestation

of the smoothed frontal- and eddy-scale SST anomalies.

Figure 10. In response to the frontal-scale SST anomalies in STFZ, the ensemble averaging zonally averaged Eady growth rate (units: $m \cdot s^{-2}$) of strong event years are averaged in (a) 140E-140W, (b) 140E-180, and (c) 180-140W distinguished from CTRL_NoNP. The similar responses to the eddy-scale SST

anomalies are in (d-f). The dotted areas passed the 95% significance t-test.
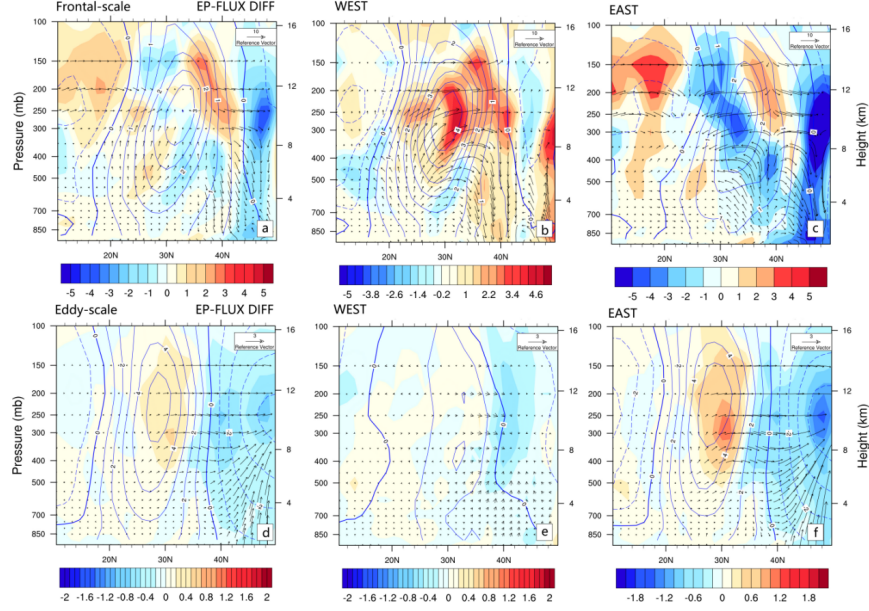
Figure 11. In response to the frontal-scale SST anomalies in STFZ, the ensemble averaging zonal wind (Contours, units: $m \cdot s^{-1}$), local E-P flux (Arrows, units: $m^2 \cdot s^{-2}$) and horizontal divergence of local E-P flux (Shadings, units: $m \cdot s^{-2}$) of strong smoothed frontal SST gradient years are zonally averaged in (a) 140E-140W, (b) 140E-180, and (c) 180-140W distinguished from CTRL_NoNP. The similar responses to the eddy-scale SST anomalies are in (d-f).

6 Conclusions

In this paper, we use Climate Forecast System Reanalysis (CFSR) high-resolution reanalysis data and numerical simulation experiments to study the influences of the multi-scale oceanic anomalies in the North Pacific in winter, including the basin-scale sea surface temperature (SST) anomaly of the North Pacific Decadal Oscillation (PDO) and its southern SST gradient, the frontal-scale smoothed SST anomaly in the subtropical front zone (STFZ) and the forcing by the spatial dispersed eddy-scale SST anomalies within the STFZ. Using regression analysis and the Liang-Kleeman information flow method, it is found that the above three kinds of oceanic forcings all correspond to the acceleration of the atmospheric upper jet over the North Pacific. The largest increment of the jet acceleration is by the basin-scale PDO-pattern SST anomaly, but similar significant results are found for the frontal-scale STFZ and the spatial dispersed eddy-scale SST anomalies within the STFZ. However, in the observation data, the three oceanic forcing sources coexist simultaneously. It is difficult to analyze their respective forcing mechanism on the atmospheric circulation.

Several sets of the Community Atmosphere Model Version 5.3 (CAM5.3) experiments are designed in this study to separate the three types of SST forcing fields. Thus, the atmospheric responses and mechanisms caused by them were quantitatively analyzed. For the positive PDO phase years, the basin-scale PDO-pattern SST cooling first causes negative mid-latitude turbulent heat flux anomalies, lower atmospheric cooling, and wind deceleration. At the same time, there is a positive lower air temperature gradient response on its south side (20°N), which causes enhanced atmospheric eddy heat transport and an atmospheric warming of 700 hPa over the cold sea surface in the following pentad. Subsequently, the warmer temperature with a new larger air temperature gradient generates on the north side leads to the even stronger poleward and upward development of baroclinic fluctuations. A positive feedback is composed by abnormal increment of northward and upward warming, accompanied larger temperature gradient to the north, enhanced poleward and upward baroclinic eddy activities, and the increased heat transport caused by eddy. Thus, it eventually causes the acceleration of the upper-level jet. The basin-scale PDO-pattern cold SST anomaly only causes the decreases of lower air temperature and the thermal wind speed in the initial stage (within 5 simulation days), through the weakened upward turbulent heat flux. This process reflects the direct forcing of initial cold sea temperature on the lower atmosphere. However, due to the temperature gradient on the south side of SST anomaly and the upward and poleward feedback process between the baroclinity and eddy heat transport proposed in this paper, the atmospheric westerly jet accelerates with equivalent barotropic structure after 10 days. The forcing of the basin-scale PDO-pattern SST anomaly on the upper atmospheric circulation mainly depends on the initial SST meridional gradient on its southern side, rather than the basin-scale SST anomaly itself.

From the above, the meridional sea temperature gradient in the STFZ induced by basin-scale PDO-pattern SST anomaly has significant forcing effects on upper jet. Hence, we conducted several numerical experiments changing the meridional SST gradient within the STFZ, including the total observed SST anomalies in the STFZ, the frontal-scale SST anomalies obtained by smoothing, and the spatial dispersed eddy-scale SST anomalies within the region. The smoothed frontal-scale and the spatial dispersed eddy-scale SST anomalies within the STFZ both appear to enhance the baroclinity of the lower atmosphere, increase the upward baroclinic atmospheric energy, and finally enhance the zonal wind of the upper layer. The simulated zonal mean atmospheric upper jet responses are comparable, though the SST anomaly is significantly stronger in the frontal-scale experiment than that in the eddy-scale experiment. However, considering the different zonal distribution characteristics of meridional temperature gradient, the simulated Eady growth rate, the uploading position and the horizontal divergence of E-P flux anomalies are different in the east-west direction between the frontal- and eddy-scale effects simulations. Therefore, the position of the upper westerly jet acceleration in the response to the eddy-scale SST anomaly is more easterly than that of the frontal-scale simulations.

Considering that the observed spatial dispersed eddy-scale SST anomalies do

not stand alone to force the upper atmosphere. We further analyzed the differences in the impacts of eddy-scale SST anomalies on the upper atmosphere under different PDO phase backgrounds. The results show that the forcing on the upper atmospheric jet by the strong eddy events in the STFZ is more significant during the positive (cold North Pacific SST anomalies) PDO phases (Supplementary Figure S4). This is due to the superposition of the meridional SST gradient both of which caused by the spatial dispersed eddy-scale SST anomalies in the STFZ region and the basin-scale SST gradient on the south side of the PDO-pattern cold SST. It can be seen that the basin-, frontal-, and eddy-scale oceanic forcing effects on the winter North Pacific jet exist simultaneously, which are of equal importance. More complex linear or even nonlinear superimposed forcing effects may exist, which is probably one of the reasons why it is difficult to detect the certain forcing of the mid-latitude oceans on the atmosphere in observations.

Acknowledgments

Open Research

The NCEP Climate Forecast System Reanalysis 6-hourly data used in this study was obtained from the website (https://rda.ucar.edu/datasets/ds093.0/index.html#cgi-bin/datasets/getWebList)

Conflicts of interest/Competing interests

The authors have no conflicts of interest to declare that are relevant to the content of this article.

Authors' contributions

Writing - original draft: Yihang Zhao and Haibo Hu

Writing - Review and Editing: Haibo Hu and Yihang Zhao

Visualization: Yihang Zhao

References

Battisti, D. S., Bhatt, U. S., & Alexander, M. A. (1995). A modeling study of the interannual variability in the wintertime North Atlantic Ocean. Journal of Climate, 8(12), 3067-3083. doi:10.1175/1520-0442(1995)008<3067:Amsoti>2.0.Co;2

Bjerknes, J. (1969). ATMOSPHERIC TELECONNECTIONS FROM EQUATORIAL PACIFIC. Monthly Weather Review, 97(3), 163-&. doi:10.1175/1520-0493(1969)097<0163:Atftep>2.3.Co;2

Carvalho, D., Rocha, A., & Gomez-Gesteira, M. (2012). Ocean surface wind simulation forced by different reanalyses: Comparison with observed data along the Iberian Peninsula coast. Ocean Modelling, 56, 31-42. doi:10.1016/j.ocemod.2012.08.002

Chelton, D. B., Schlax, M. G., Samelson, R. M., & de Szoeke, R. A. (2007). Global observations of large oceanic eddies. Geophysical Research Letters, 34(15). doi:10.1029/2007gl030812

Chen, Q. Y., Hu, H. B., Ren, X. J., & Yang, X. Q. (2019). Numerical Simulation of Midlatitude Upper-Level Zonal Wind Response to the Change of North Pacific Subtropical Front Strength. Journal of Geophysical Research-Atmospheres, 124(9), 4891-4912. doi:10.1029/2018jd029589

Chu, C. J., Yang, X. Q., Ren, X. J., & Zhou, T. J. (2013). Response of Northern Hemisphere storm tracks to Indian-western Pacific Ocean warming in atmospheric general circulation models. Climate Dynamics, 40(5-6), 1057-1070. doi:10.1007/s00382-013-1687-y

Deser, C., & Timlin, M. S. (1997). Atmosphere-ocean interaction on weekly timescales in the North Atlantic and Pacific. Journal of Climate, 10(3), 393-408. doi:10.1175/1520-0442(1997)010<0393:Aoiowt>2.0.Co;2

Feliks, Y., Ghil, M., & Simonnet, E. (2004). Low-frequency variability in the midlatitude atmosphere induced by an oceanic thermal front. Journal of the Atmospheric Sciences, 61(9), 961-981. doi:10.1175/1520-0469(2004)061<0961:Lvitma>2.0.Co;2

Feliks, Y., Ghil, M., & Simonnet, E. (2007). Low-frequency variability in the midlatitude baroclinic atmosphere induced by an oceanic thermal front. Journal of the Atmospheric Sciences, 64(1), 97-116. doi:10.1175/jas3780.1

Frankignoul, C., Muller, P., & Zorita, E. (1997). A simple model of the decadal response of the ocean to stochastic wind forcing. Journal of Physical Oceanography, 27(8), 1533-1546. doi:10.1175/1520-0485(1997)027<1533:Asmotd>2.0.Co;2

Gent, P. R., Danabasoglu, G., Donner, L. J., Holland, M. M., Hunke, E. C., Jayne, S. R., . . . Zhang, M. H. (2011). The Community Climate System Model Version 4. Journal of Climate, 24(19), 4973-4991. doi:10.1175/2011jcli4083.1

Hasselmann, K. (1976). STOCHASTIC CLIMATE MODELS .1. THEORY. Tellus, 28(6), 473-485. doi:10.1111/j.2153-3490.1976.tb00696.x

Hoskins, B. J., & Karoly, D. J. (1981). THE STEADY LINEAR RESPONSE OF A SPHERICAL ATMOSPHERE TO THERMAL AND

OROGRAPHIC FORCING. Journal of the Atmospheric Sciences, 38(6), 1179-1196. doi:10.1175/1520-0469(1981)038<1179:Tslroa>2.0.Co;2

Hu, H. B., Zhao, Y. H., Zhang, N., Bai, H. K., & Chen, F. F. (2021). Local and remote forcing effects of oceanic eddies in the subtropical front zone on the mid-latitude atmosphere in Winter. Climate Dynamics, 57(11-12), 3447-3464. doi:10.1007/s00382-021-05877-8

Jiang, S., Hu, H., Zhang, N., Lei, L., & Bai, H. (2019). Multi-source forcing effects analysis using Liang–Kleeman information flow method and the community atmosphere model (CAM4.0). Climate Dynamics, 53(9), 6035-6053. doi:10.1007/s00382-019-04914-x

Jin, F. F. (1997). An equatorial ocean recharge paradigm for ENSO .1. Conceptual model. Journal of the Atmospheric Sciences, 54(7), 811-829. doi:10.1175/1520-0469(1997)054<0811:Aeorpf>2.0.Co;2

Kushnir, Y., & Held, I. M. (1996). Equilibrium atmospheric response to North Atlantic SST anomalies. Journal of Climate, 9(6), 1208-1220. doi:10.1175/1520-0442(1996)009<1208:Eartna>2.0.Co;2

Kushnir, Y., & Lau, N. C. (1992). THE GENERAL-CIRCULATION MODEL RESPONSE TO A NORTH PACIFIC SST ANOMALY - DEPENDENCE ON TIME SCALE AND PATTERN POLARITY. Journal of Climate, 5(4), 271-283. doi:10.1175/1520-0442(1992)005<0271:Tgcmrt>2.0.Co;2

Larkin, N. K., & Harrison, D. E. (2002). ENSO warm (El Nino) and cold (La Nina) event life cycles: Ocean surface anomaly patterns, their symmetries, asymmetries, and implications. Journal of Climate, 15(10), 1118-1140. doi:10.1175/1520-0442(2002)015<1118:Ewenoa>2.0.Co;2

Latif, M., & Barnett, T. P. (1996). Decadal climate variability over the North Pacific and North America: Dynamics and predictability. Journal of Climate, 9(10), 2407-2423. doi:10.1175/1520-0442(1996)009<2407:Dcvotn>2.0.Co;2

Liang, X. S. (2013). Local predictability and information flow in complex dynamical systems. Physica D-Nonlinear Phenomena, 248, 1-15. doi:10.1016/j.physd.2012.12.011

Liang, X. S. (2014). Unraveling the cause-effect relation between time series. Physical Review E, 90(5). doi:10.1103/PhysRevE.90.052150

Liang, X. S. (2015). Normalizing the causality between time series. Physical Review E, 92(2). doi:10.1103/PhysRevE.92.022126

Liang, X. S. (2016). Information flow and causality as rigorous notions ab initio. Physical Review E, 94(5). doi:10.1103/PhysRevE.94.052201

Liu, Z. Y. (2012). Dynamics of Interdecadal Climate Variability: A Historical Perspective. Journal of Climate, 25(6), 1963-1995. doi:10.1175/2011jcli3980.1

Liu, Z. Y., & Wu, L. X. (2004). Atmospheric response to North Pacific SST: The role of ocean-atmosphere coupling. Journal of Climate, 17(9), 1859-1882. doi:10.1175/1520-0442(2004)017<1859:Artnps>2.0.Co;2

Ma, J., Xu, H. M., Dong, C. M., Lin, P. F., & Liu, Y. (2015). Atmospheric responses to oceanic eddies in the Kuroshio Extension region. Journal of Geophysical Research-Atmospheres, 120(13), 6313-6330. doi:10.1002/2014jd022930

Ma, X. H., Chang, P., Saravanan, R., Montuoro, R., Hsieh, J. S., Wu, D. X., . . . Jing, Z. (2015). Distant Influence of Kuroshio Eddies on North Pacific Weather Patterns? Scientific Reports, 5. doi:10.1038/srep17785

Mantua, N. J., & Hare, S. R. (2002). The Pacific decadal oscillation. Journal of Oceanography, 58(1), 35-44. doi:10.1023/a:1015820616384

Mantua, N. J., Hare, S. R., Zhang, Y., Wallace, J. M., & Francis, R. C. (1997). A Pacific interdecadal climate oscillation with impacts on salmon production. Bulletin of the American Meteorological Society, 78(6), 1069-1079. doi:10.1175/1520-0477(1997)078<1069:Apicow>2.0.Co;2

Miller, A. J., & Schneider, N. (2000). Interdecadal climate regime dynamics in the North Pacific Ocean: theories, observations and ecosystem impacts. Progress in Oceanography, 47(2-4), 355-379. doi:10.1016/s0079-6611(00)00044-6

Nakamura, H., Lin, G., & Yamagata, T. (1997). Decadal climate variability in the North Pacific during the recent decades. Bulletin of the American Meteorological Society, 78(10), 2215-2225. doi:10.1175/1520-0477(1997)078<2215:Dcvitn>2.0.Co;2

Neale, R. B., Richter, J. H., & Jochum, M. (2008). The Impact of Convection on ENSO: From a Delayed Oscillator to a Series of Events. Journal of Climate, 21(22), 5904-5924. doi:10.1175/2008jcli2244.1

Newman, M., Alexander, M. A., Ault, T. R., Cobb, K. M., Deser, C., Di Lorenzo, E., . . . Smith, C. A. (2016). The Pacific Decadal Oscillation, Revisited. Journal of Climate, 29(12), 4399-4427. doi:10.1175/jcli-d-15-0508.1

Palmer, T. N., & Zhaobo, S. (1985). A MODELING AND OBSERVATIONAL STUDY OF THE RELATIONSHIP BETWEEN SEA-SURFACE TEMPERATURE IN THE NORTHWEST ATLANTIC AND THE ATMOSPHERIC GENERAL-CIRCULATION. Quarterly Journal of the Royal Meteorological Society, 111(470), 947-975. doi:10.1256/smsqj.47002

Peng, S. L., & Whitaker, J. S. (1999). Mechanisms determining the atmospheric response to midlatitude SST anomalies. Journal of Climate, 12(5), 1393-1408. doi:10.1175/1520-0442(1999)012<1393:Mdtart>2.0.Co;2

Philander, S. G. H. (1983). EL-NINO SOUTHERN OSCILLATION PHENOMENA. Nature, 302(5906), 295-301. doi:10.1038/302295a0

Rasmusson, E. M., & Wallace, J. M. (1983). METEOROLOGICAL ASPECTS OF THE EL-NINO SOUTHERN OSCILLATION. Science, 222(4629), 1195-1202. doi:10.1126/science.222.4629.1195

Ren, X. J., Yang, X. Q., & Chu, C. J. (2010). Seasonal Variations of the Synoptic-Scale Transient Eddy Activity and Polar Front Jet over East Asia. Journal of Climate, 23(12), 3222-3233. doi:10.1175/2009jcli3225.1

Richter, J. H., & Rasch, P. J. (2008). Effects of convective momentum transport on the atmospheric circulation in the community atmosphere model, version 3. Journal of Climate, 21(7), 1487-1499. doi:10.1175/2007jcli1789.1

Sampe, T., Nakamura, H., Goto, A., & Ohfuchi, W. (2010). Significance of a Midlatitude SST Frontal Zone in the Formation of a Storm Track and an Eddy-Driven Westerly Jet. Journal of Climate, 23(7), 1793-1814. doi:10.1175/2009jcli3163.1

San Liang, X. (2018). Causation and information flow with respect to relative entropy. Chaos, 28(7). doi:10.1063/1.5010253

Small, R. J., deSzoeke, S. P., Xie, S. P., O'Neill, L., Seo, H., Song, Q., . . . Minobe, S. (2008). Air-sea interaction over ocean fronts and eddies. Dynamics of Atmospheres and Oceans, 45(3-4), 274-319. doi:10.1016/j.dynatmoce.2008.01.001

Stips, A., Macias, D., Coughlan, C., Garcia-Gorriz, E., & San Liang, X. (2016). On the causal structure between CO_2 and global temperature. Scientific Reports, 6. doi:10.1038/srep21691

Sun, X. G., Tao, L. F., & Yang, X. Q. (2018). The Influence of Oceanic Stochastic Forcing on the Atmospheric Response to Midlatitude North Pacific SST Anomalies. Geophysical Research Letters, 45(17), 9297-9304. doi:10.1029/2018gl078860

Sutton, R., & Mathieu, P. P. (2002). Response of the atmosphere-ocean mixed-layer system to anomalous ocean heat-flux convergence. Quarterly Journal of the Royal Meteorological Society, 128(582), 1259-1275. doi:10.1256/003590002320373283

Szunyogh, I., Forinash, E., Gyarmati, G., Jia, Y. L., Chang, P., & Saravanan, R. (2021). Evaluation of a Coupled Modeling Approach for the Investigation of the Effects of SST Mesoscale Variability on the Atmosphere. Journal of Advances in Modeling Earth Systems, 13(9). doi:10.1029/2020ms002412

Trenberth, K. E. (1986). An Assessment of the Impact of Transient Eddies on the Zonal Flow during a Blocking Episode Using Localized Eliassen-Palm Flux Diagnostics, Journal of Atmospheric Sciences, 43(19), 2070-2087. doi:10.1175/1520-0469(1986)043<2070:AAOTIO>2.0.CO;2

Wang, L. Y., Hu, H. B., & Yang, X. Q. (2019). The atmospheric responses to the intensity variability of subtropical front in the wintertime North Pacific.

Climate Dynamics, 52(9-10), 5623-5639. doi:10.1007/s00382-018-4468-9

Wang, L. Y., Hu, H. B., Yang, X. Q., & Ren, X. J. (2016). Atmospheric eddy anomalies associated with the wintertime North Pacific subtropical front strength and their influences on the seasonal-mean atmosphere. Science China-Earth Sciences, 59(10), 2022-2036. doi:10.1007/s11430-016-5331-7

Wen, Z. B., Hu, H. B., Song, Z. Y., Bai, H. K., & Wang, Z. Y. (2020). Different Influences of Mesoscale Oceanic Eddies on the North Pacific Subsurface Low Potential Vorticity Water Mass Between Winter and Summer. Journal of Geophysical Research-Oceans, 125(1). doi:10.1029/2019jc015333

Wu, L. X., & Liu, Z. G. (2003). Decadal variability in the North Pacific: The eastern North Pacific mode. Journal of Climate, 16(19), 3111-3131. doi:10.1175/1520-0442(2003)016<3111:Dvitnp>2.0.Co;2

Xu, L. X., Li, P. L., Xie, S. P., Liu, Q. Y., Liu, C., & Gao, W. D. (2016). Observing mesoscale eddy effects on mode-water subduction and transport in the North Pacific. Nature Communications, 7. doi:10.1038/ncomms10505

Xue, Y., Huang, B. Y., Hu, Z. Z., Kumar, A., Wen, C. H., Behringer, D., & Nadiga, S. (2011). An assessment of oceanic variability in the NCEP climate forecast system reanalysis. Climate Dynamics, 37(11-12), 2511-2539. doi:10.1007/s00382-010-0954-4

Yao, Y., Zhong, Z., & Yang, X. Q. (2016). Numerical experiments of the storm track sensitivity to oceanic frontal strength within the Kuroshio/Oyashio Extensions. Journal of Geophysical Research-Atmospheres, 121(6), 2888-2900. doi:10.1002/2015jd024381

Yulaeva, E., Schneider, N., Pierce, D. W., & Barnett, T. P. (2001). Modeling of North Pacific climate variability forced by oceanic heat flux anomalies. Journal of Climate, 14(20), 4027-4046. doi:10.1175/1520-0442(2001)014<4027:Monpcv>2.0.Co;2

Zhang, G. J., & McFarlane, N. A. (1995). SENSITIVITY OF CLIMATE SIMULATIONS TO THE PARAMETERIZATION OF CUMULUS CONVECTION IN THE CANADIAN CLIMATE CENTER GENERAL-CIRCULATION MODEL. Atmosphere-Ocean, 33(3), 407-446. doi:10.1080/07055900.1995.9649539